Electronic Supplementary Material (ESI) for Journal of Materials Chemistry A.

Silica direct evaporation: A size-controlled approach to SiC/carbon nanosheet composites as Pt catalyst support for superior methanol electrooxidation

Lei Wang,[a] Lu Zhao,[a] Peng Yu,[a] Chungui Tian,[a] Fanfei Sun,[b] He Feng,[a] Wei Zhou,[a] Jianqiang Wang,[b] Honggang Fu[a,*]

[a] *Key Laboratory of Functional Inorganic Material Chemistry, Ministry of Education of the People' s Republic of China, Heilongjiang University, Harbin 150080 (P. R. China); Fax: (+86) 451-8666-1259; E-mail: fuhg@vip.sina.com*

[b] *Shanghai Synchrotron Radiation Facility (SSRF), Shanghai Institute of Applied Physics, Chinese Academy of Sciences, Shanghai, 201204, P. R. China*

Table S1. The synthetic conditions for all the compared samples.

Samples	Synthetic conditions	Heating temperature (^{o}C)
SiC/GC (also called as SiC/GC-1400)	ceramic chip	1400
SiC/GC-1300	ceramic chip	1300
SiC/GC-1500	ceramic chip	1500
GC	without ceramic chip	1400
SiC/C	The CS without treating by $FeCl_3$	1400

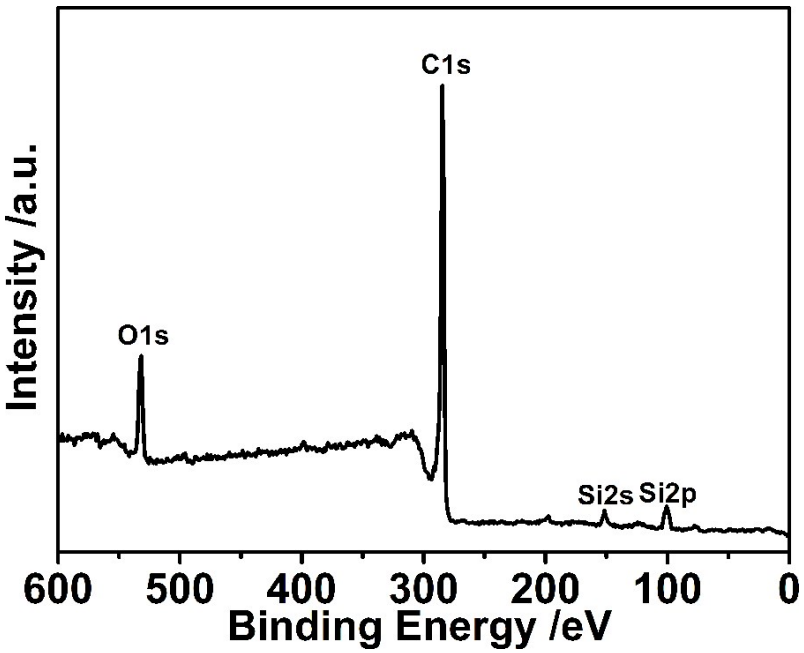

Fig. S1 Wide XPS spectrum of SiC/GC composite.

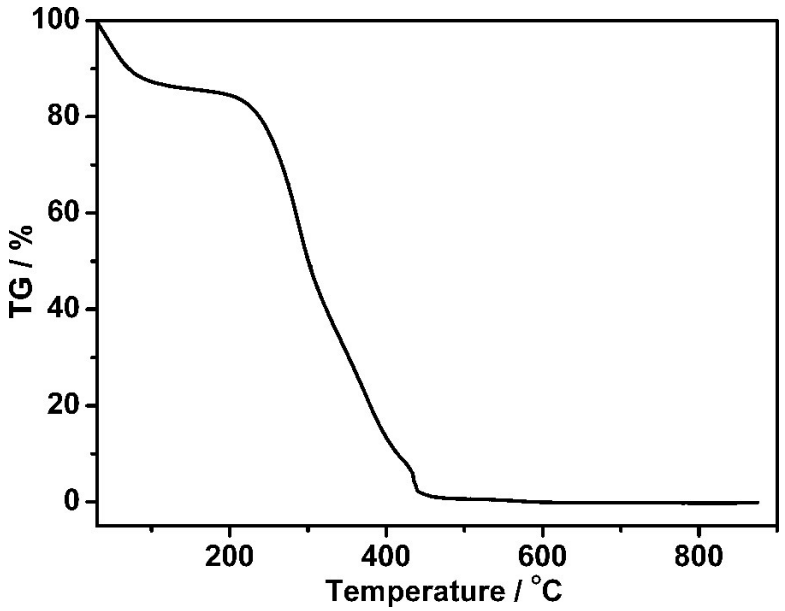

Fig. S2 TG analysis of CS raw material under air.

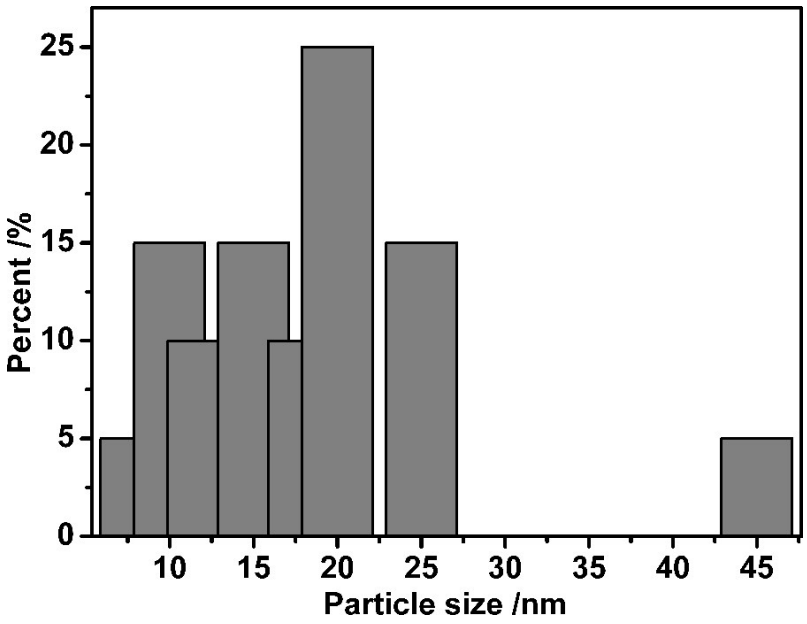

Fig. S3 The corresponding Pt NPs size-distributed graph calculated from Fig. 2A.

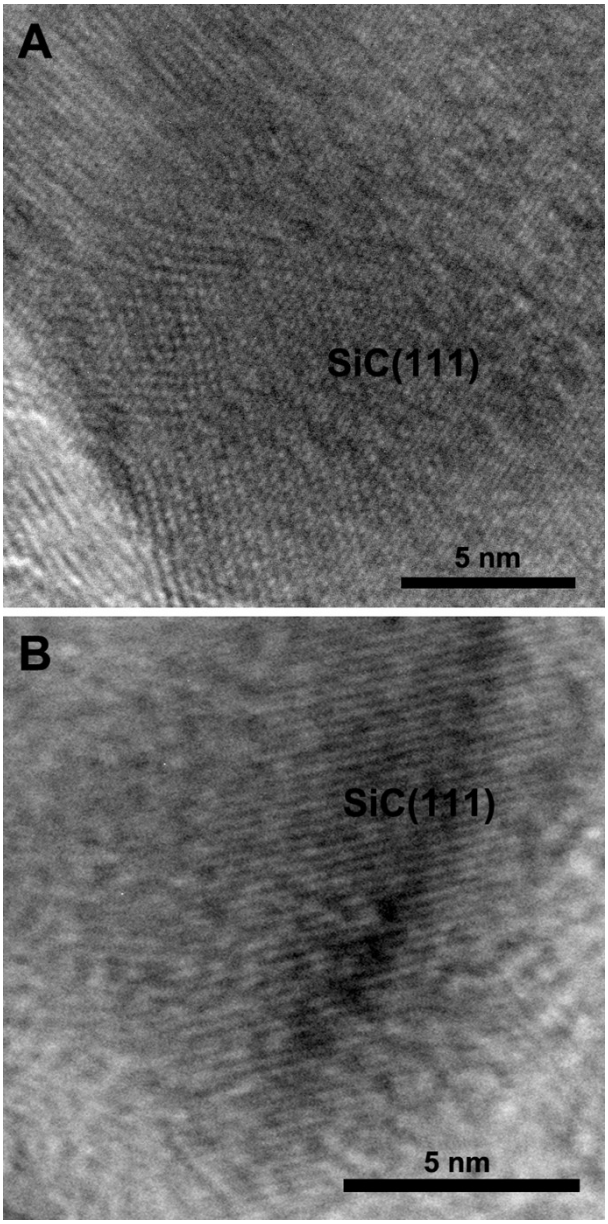

Fig. S4 A, B are the corresponding HRTEM images of Fig. 2C and Fig. 2D, respectively.

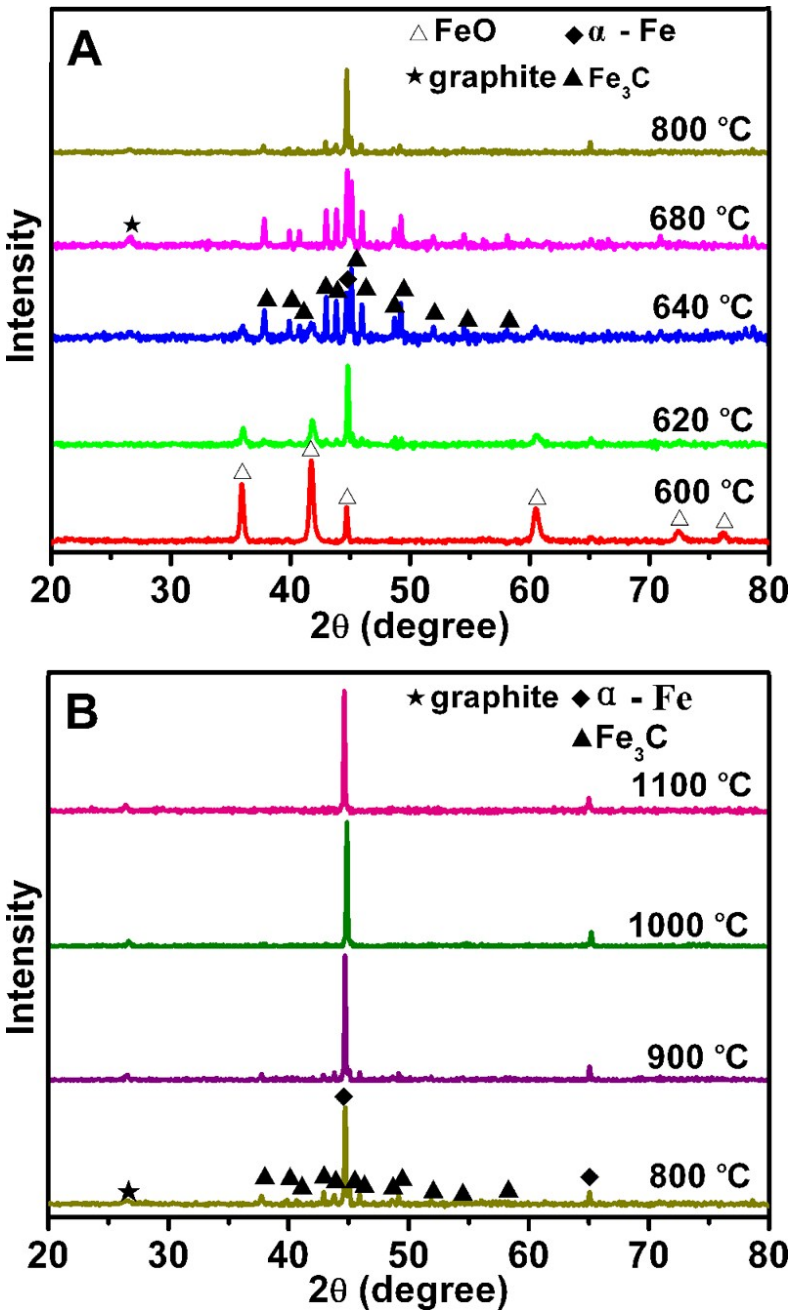

Fig. **S5** XRD patterns of the composites derived from CS-Fe^{3+} precursor with the heating temperature of 600~1100 °C.

Table S2. Fitting parameters of the Fe EXAFS spectra based on Fig. 3.

Heating temperature	Shell	N [a]	R (Å) [b]
600°C	Fe-O	2.8±0.5	2.06±0.02
	Fe-Fe	11.0±1.1	3.06±0.01
	Fe-Fe	8.3±1.1	4.33±0.03
620°C	Fe-C/O	2.2±0.2	2.08±0.02
	Fe-Fe	2.1±0.4	2.52±0.01
	Fe-Fe	5.2±0.6	3.12±0.05
680°C	Fe-C	0.4±0.1	1.87±0.02
	Fe-Fe	7.2±0.4	2.51±0.01
	Fe-Fe	9.3±1.7	4.07±0.01
800°C	Fe-Fe	3.1±0.4	2.43±0.01
	Fe-Fe	2.5±0.3	2.81±0.01
	Fe-Fe	6.3±0.4	4.06±0.01

[a] Coordination number. [b] Distance between absorber and backscatterer atoms.

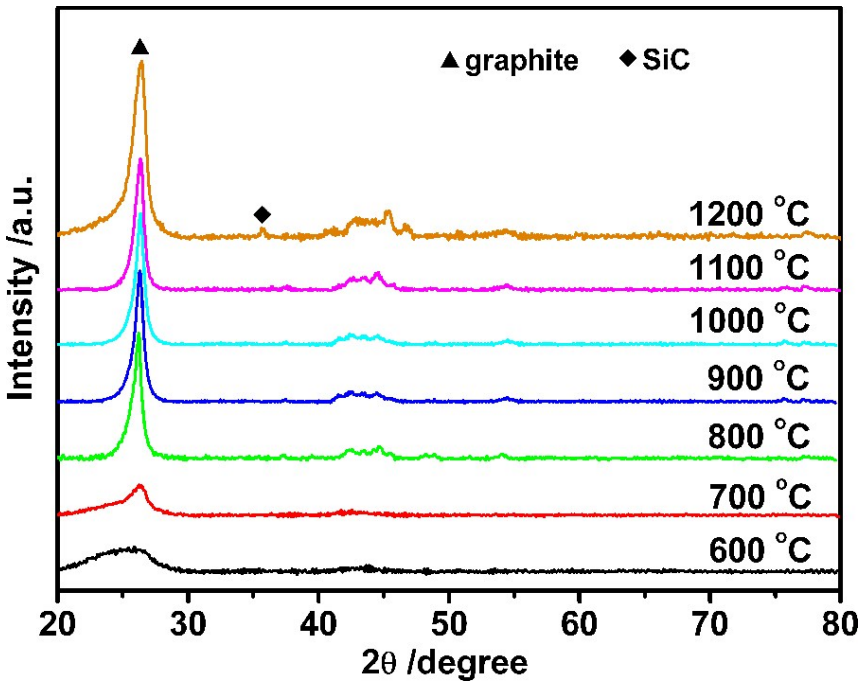

Fig. S6 XRD patterns of the samples derived from CS-Fe^{3+} precursor with the heating temperature of 600~1200 °C after treating with 10 % HCl.

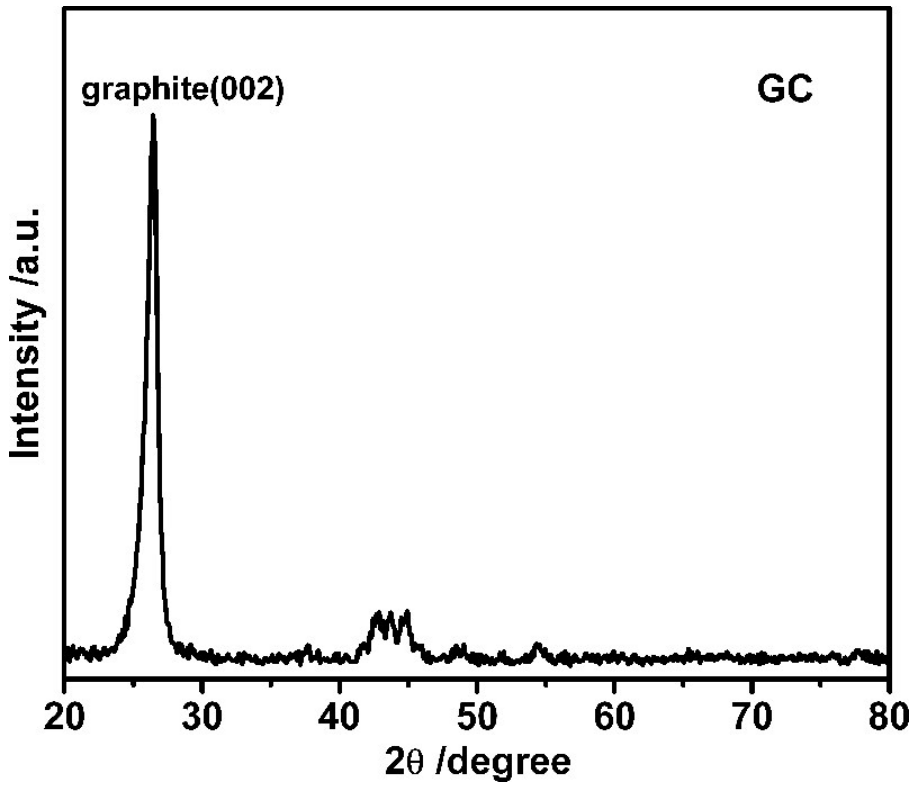

Fig. S7 XRD pattern of GC synthesized from coconut-Fe^{3+} precursor without ceramic chip at a heating temperature of 1400 ^{o}C.

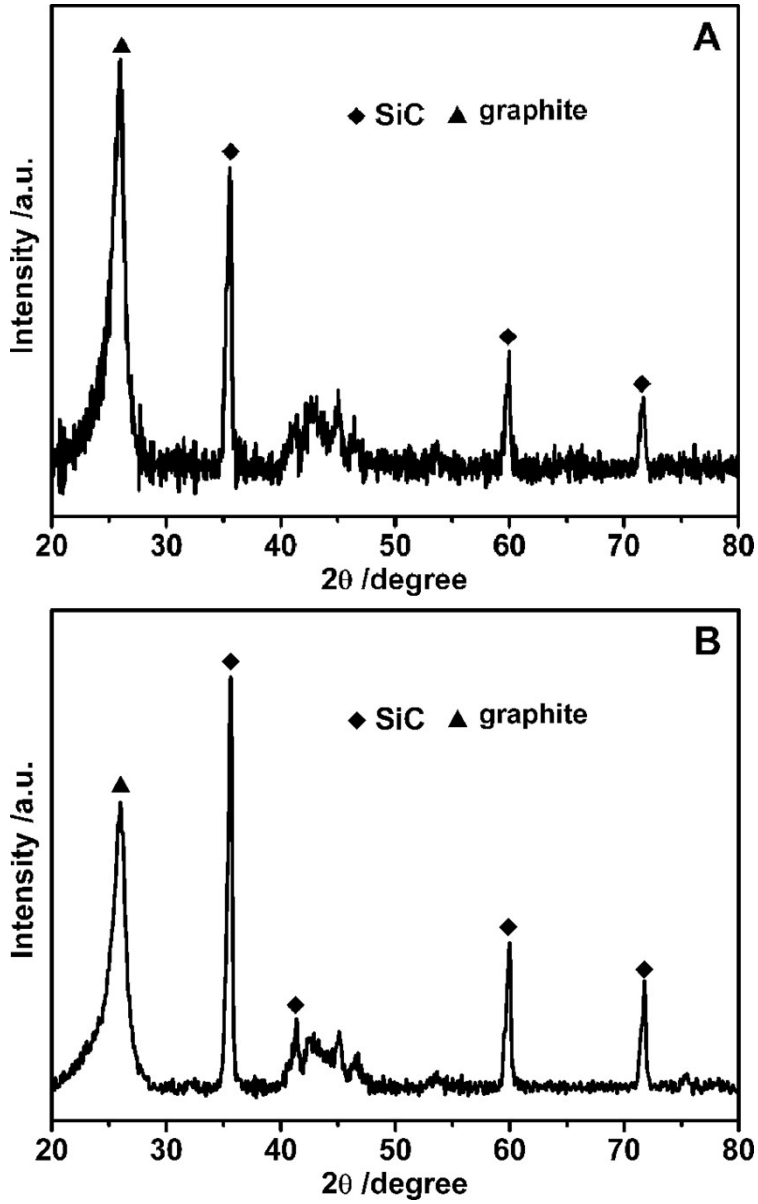

Fig. S8 XRD patterns of (A) SiC/GC-1300 and (B) SiC/GC-1500, respectively.

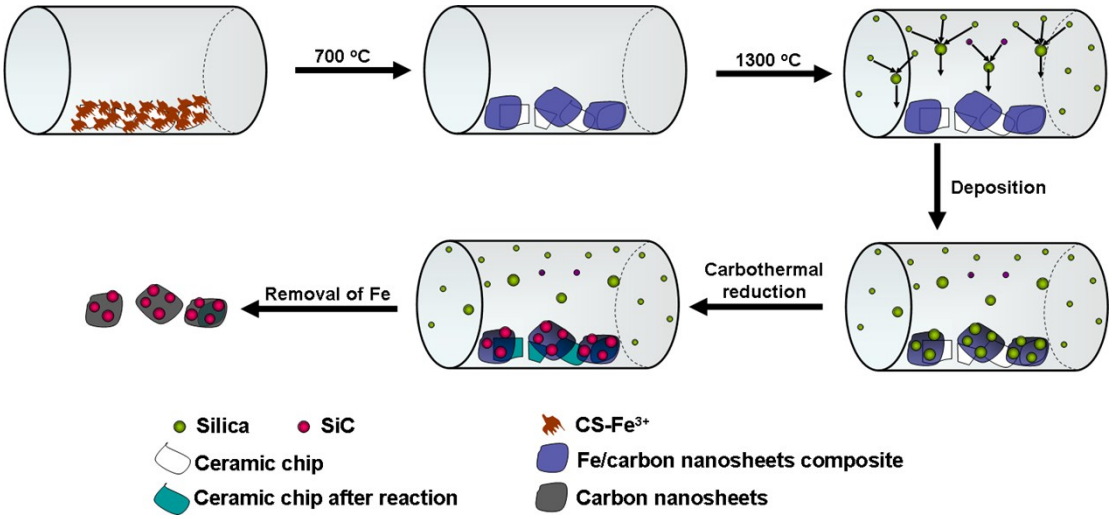

Scheme S1. The supposed formation process of SiC/GC composites synthesized from 1300 °C.

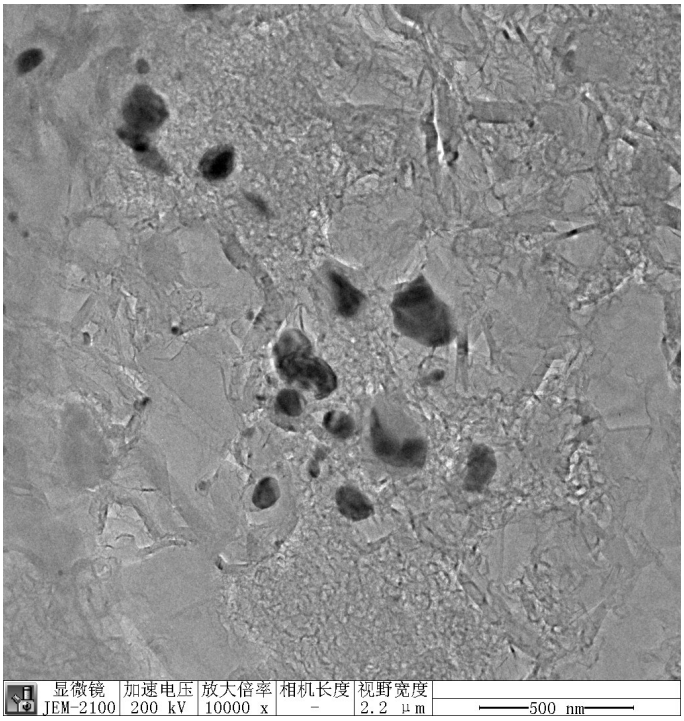

Fig. S9 TEM images of SiC/GC-1300.

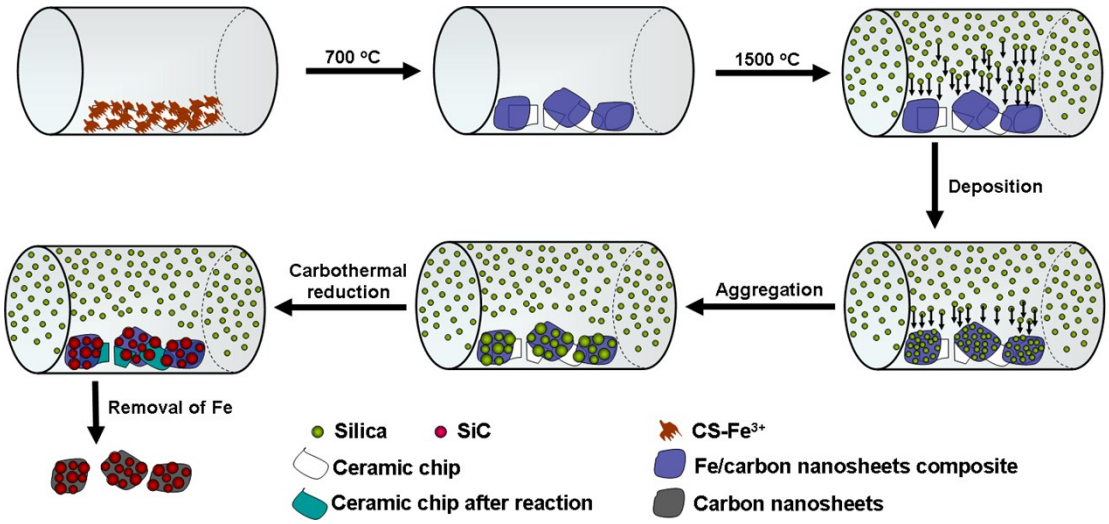

Scheme S2. The supposed formation process of SiC/GC composites synthesized from 1500 °C.

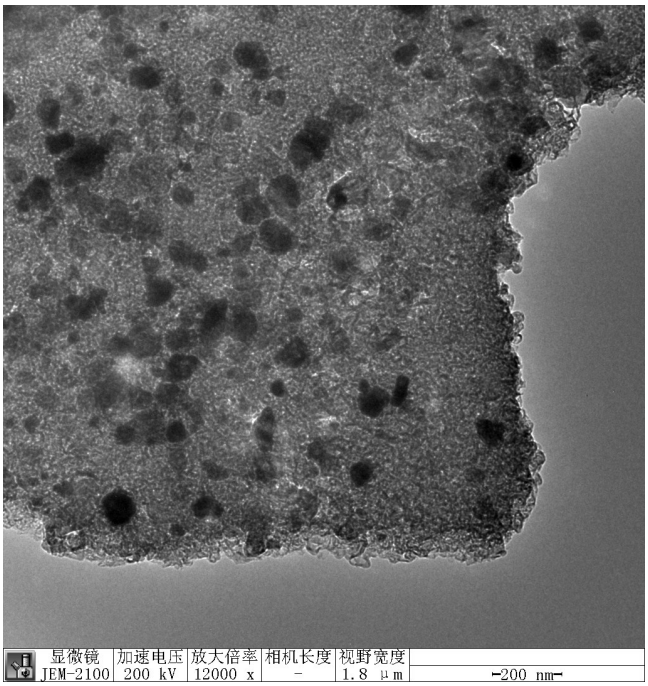

Fig. S10 TEM images of SiC/GC-1500.

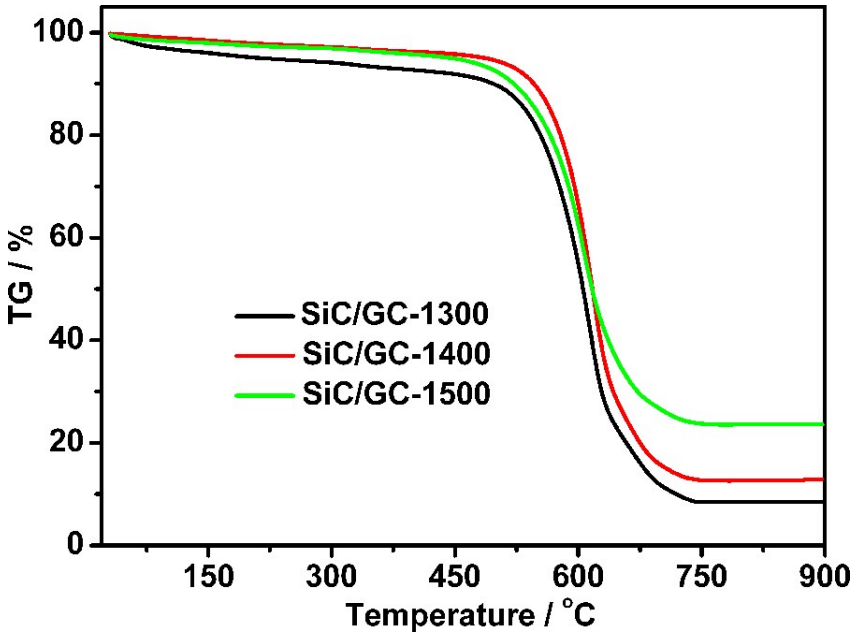

Fig. S11 TG curves of the SiC/GC samples under air synthesized from different temperatures. Notably, SiC/GC-1400 is also called as SiC/GC in this work.

Table S3. SiC content of the SiC/GC samples based on Fig. S11.

Samples	SiC content calculated from TG curves (%)
SiC/GC-1300	5.6
SiC/GC-1400 (SiC/GC)	8.4
SiC/GC-1500	16.1

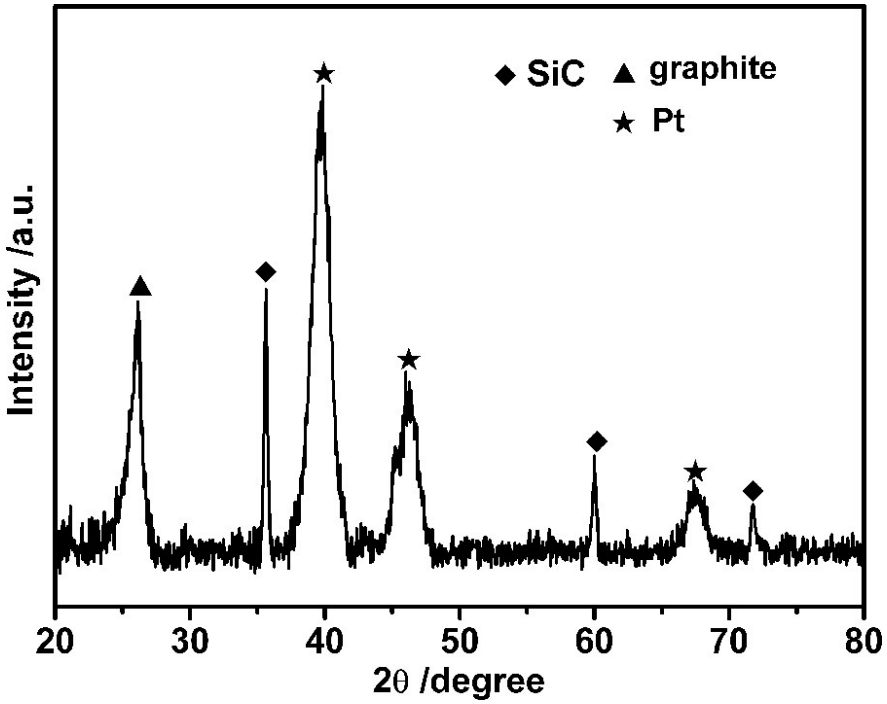

Fig. S12 XRD pattern of Pt-SiC/GC composite.

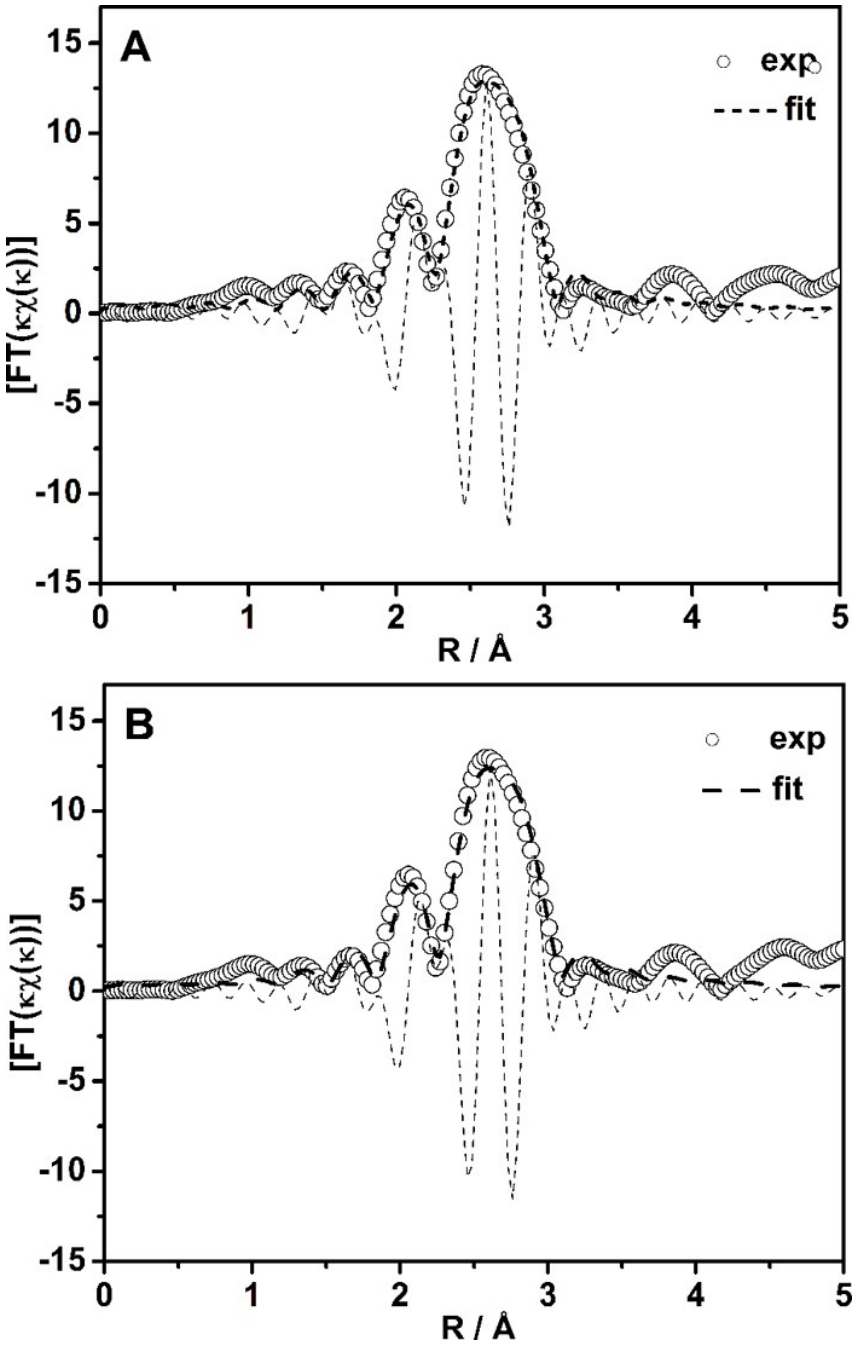

Fig. S13 Fourier transforms of experimental data (o) and fit data (—) of Pt L3-edge extended X-ray absorption fine structure (EXAFS) spectra for Pt-SiC/GC and Pt/GC composites.

Table S4. Fitting parameters of EXAFS spectra for Pt foil, Pt /GC and Pt-SiC/GC in Figure 5B.

Sample	shell	N[a]	R[b]	σ^2 (10^{-3} Å^2)[c]	ΔE_0 (eV)[d]
Pt foil	Pt-Pt	9.84 ± 0.8	2.76 ± 0.02	4.5 ±0.2	7.82 ± 0.4
Pt/GC	Pt-C	1.15± 0.2	2.05± 0.3	2.1± 0.4	15.8± 0.6
	Pt-Pt	8.28± 0.1	2.82± 0.06	6.3± 0.7	9.72±1.4
P-SiC/GC	Pt-C	2.04 ± 0.5	2.13± 0.04	2.6± 3.0	9.48± 0.1
	Pt-Pt	9.22± 0.2	2.75± 0.06	0.6± 0.1	8.12± 0.9

[a] Coordination number. [b] Distance between absorber and backscatterer atoms. [c] Debye–Waller factor. [d] Inner potential correction. Error bounds (accuracies) characterizing the structural parameters obtained by EXAFS spectroscopy are estimated as follows: coordination number N±20%; distance R±0.02, Debye–Waller factor σ^2±10%; and inner potential correction ΔE_0±20%.

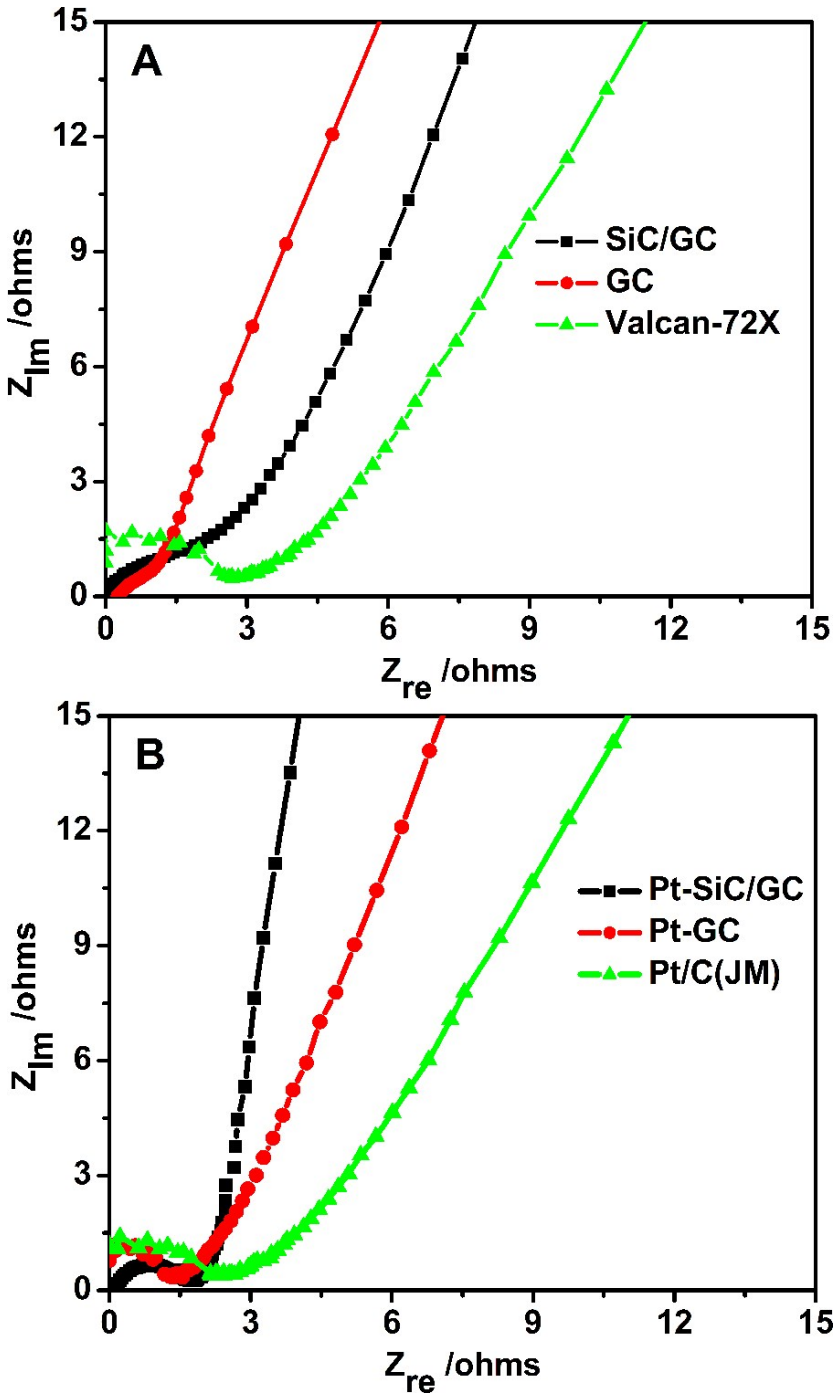

Fig. S14 Electrochemical impedance spectra (EIS) of (A) SiC/GC, GC, Vulcan-72X supports, and (B) Pt-SiC/GC, Pt/GC, Pt/C catalysts tested in 0.5 M H_2SO_4 + 0.5 M CH_3OH electrolyte.

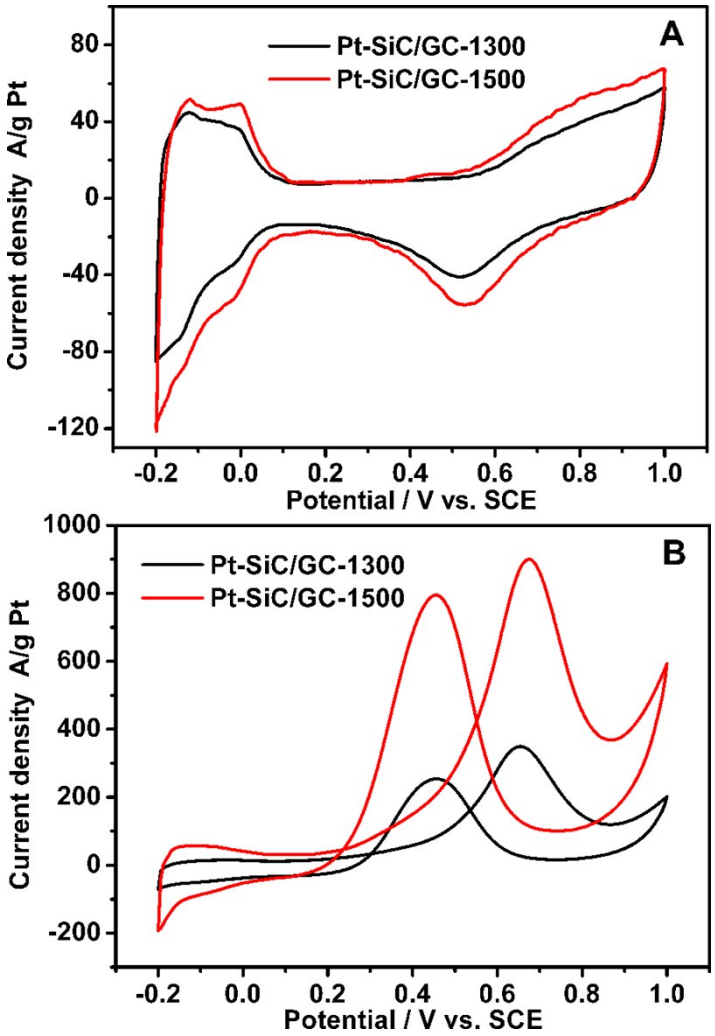

Fig. S15 Electrochemical performances of Pt-SiC/GC-1300 and Pt-SiC/GC-1500 catalysts: The CV curves in 0.5 M H_2SO_4 electrolyte (A) and 0.5 M H_2SO_4 + 0.5 M CH_3OH electrolyte (B), respectively.

Table S5 The electrochemical performance of the catalysts.

Catalysts	ECSA (A/g Pt)	Peak potential (V)	Mass current density (A/g Pt)	I_f/I_b
Pt-SiC/GC-1300	61.9	0.67	353.8	1.32
Pt-SiC/GC-1500	74.5	0.68	902.3	1.11
Pt-SiC/C	52.3	0.70	217.1	0.89

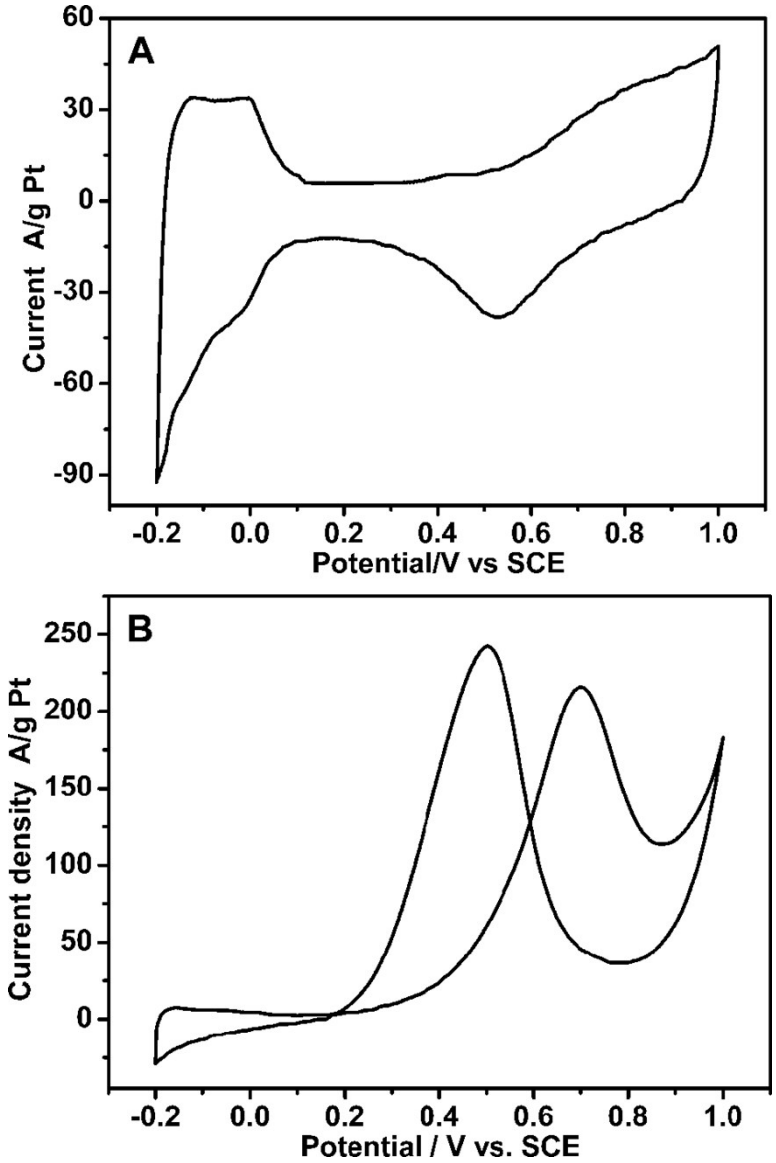

Fig. S16 The CV curves of Pt-SiC/C catalyst in (A) 0.5 M H_2SO_4 electrolyte and (B) 0.5 M H_2SO_4 + 0.5 M CH_3OH electrolyte, respectively.

Table S6. The performances of the previous reported carbide (nitride)-based Pt catalysts towards MOR.

No.	Material name	Pt content	ECSA (m^2/g Pt)	Current density (A/g Pt)	Ref.
1	Pt/SiC	32.8 %		42.25	S1
2	Pt–Ti/SiC	32.8 %	107.64	327.84	S1
3	Pt-SiC/porous carbon	20 %	62.5	836.93	S2
4	Pt/SiC		87.9	1008.3	S3
5	Pt-WC/RGO	5.7 %	253.12	888.8	S4
6	Pt-WC/mesoporous carbon	20 %		784	S5
7	Pt-WC/ordered mesoporous carbon	20 %		367.5	S6
8	Pt-WC/GC	7.5 %		205.6	S7
9	Pt-WC/GC	20.5 %	207.4	1590	S8
10	Pt-WC/GC	37.2 %		1191.8	S9
11	Pt-WC/graphene	7.5 %	103.8	686.6	S10
12	Pt–MoC–GC	36.6 %	55.1	1596.7	S11
13	Pt/NbC nanowires		72.86	766.1	S12
14	P-VC_x/C	34.9 %		~1270	S13
15	Pt/CrN	20 %	82	195	S14
16	Pt/TiC nanowires	19.7 %		348.3	S15
17	Pt–WN/graphene	7.5 %	88.4	531.5	S16
18	**Pt-SiC/GC**	**10 %**	**147.1**	**1585.3**	**This work**

References in here:

S1. Y. Zhang, J. Zang, L. Dong, X. Cheng, Y. Zhao, Y. Wang. *J. Mater. Chem. A*, **2014**, 2, 10146–10153.

S2. L. Jiang, H. Fu, L. Wang, W. Zhou, B. Jiang, R. Wang. *RSC Adv.*, **2014**, 4,

51272–51279.

S3. L. Dong, X. Tong, Y. Wang, X. Guo, G. Jin, X. Guo. *J Solid State Electrochem*, **2014**, 18, 929–934.

S4. C. Ma, W. Liu, M. Shi, X. Lang, Y. Chu, Z. Chen, D. Zhao, W. Lin, C. HardacrebaState. *Electrochimica Acta*, **2013**, 114, 133–141.

S5. Y. Wang, C. He, A. Brouzgou, Y. Liang, R. Fu, D. Wu, P. Tsiakaras, S. Song. *J. Power Sources*, **2012**, 200, 8–13.

S6. K. Wang, Y. Wang, Z. Liang, Y. Liang, D. Wu, S. Song, P. Tsiakaras. *Applied Catalysis B: Environmental*, **2014**, 147, 518–525.

S7. Wang, R. H.; Tian, C. G.; Wang, L.; Wang, B. L.; Zhang, H. B.; Fu, H. G. *Chem. Commun.* **2009**, 3104–3106.

S8. C. He, H. Meng, X. Yao, P. K. Shen. *International. J. Hydrogen Energy*, **2012**, 37, 8154–8160.

S9. Z. Yan, H. Meng, P. K. Shen, R. Wang, L. Wang, K. Shi, H. Fu. *J. Mater. Chem.*, **2012**, 22, 5072–5079.

S10. R. Wang, Y. Xie, K. Shi, J. Wang, C. Tian, P. Shen, H. Fu. *Chem. Eur. J.*, **2012**, 18, 7443–7451.

S11. Z. Yan, G. He, P. K. Shen, Z. Luo, J. Xie, M. Chen. *J. Mater. Chem. A*, **2014**, 2, 4014–4022.

S12. Z. Qiu, H. Huang, J. Du, T. Feng, W. Zhang, Y. Gan, X. Tao. *J. Phys. Chem. C*, **2013**, 117, 13770–13775.

S13. Z. Yan, M. Cai, P. K. Shen. *J. Mater. Chem.*, **2011**, 21, 19166–19170.

S14. M. Yang, R. Guarecuco, F. J. DiSalvo. *Chem. Mater.*, **2013**, 25, 1783−1787.

S15. Z. Qiu, H. Huang, J. Du, X. Tao, Y. Xia, T. Feng, Y. Gan, W. Zhang. *J. Mater. Chem. A,* **2014**, 2, 8003–8008.

S16. H. Yan, C. Tian, L. Sun, B. Wang, L. Wang, J. Yin, A. Wu, H. Fu. *Energy Environ. Sci.*, **2014**, 7, 1939–1949.